Biomimetic Intelligence and Robotics 4 (2024) 100185

Contents lists available at ScienceDirect

Biomimetic Intelligence and Robotics

journal homepage: www.elsevier.com/locate/birob

Research Article

LQR-based control strategy for improving human–robot companionship and natural obstacle avoidance

Zefan Su [a,b], Hanchen Yao [b], Jianwei Peng [b], Zhelin Liao [b], Zengwei Wang [c], Hui Yu [b,*], Houde Dai [b,*], Tim C. Lueth [c]

[a] School of Advanced Manufacturing, Fuzhou University, Jinjiang 362251, China
[b] Quanzhou Institute of Equipment Manufacturing, Fujian Institute of Research on the Structure of Matter, Chinese Academy of Sciences, Jinjiang 362200, China
[c] Institute of Micro Technology and Medical Device Technology (MIMED), School of Engineering and Design, Technical University of Munich, Garching 85748, Germany

ARTICLE INFO

Article history:
Received 29 June 2024
Revised 18 August 2024
Accepted 20 September 2024
Available online 4 October 2024

Keywords:
Human–robot interaction
Linear quadratic regulator
Human-accompanying robots
Behavioral dynamics

ABSTRACT

In the dynamic and unstructured environment of human–robot symbiosis, companion robots require natural human–robot interaction and autonomous intelligence through multimodal information fusion to achieve effective collaboration. Nevertheless, the control precision and coordination of the accompanying actions are not satisfactory in practical applications. This is primarily attributed to the difficulties in the motion coordination between the accompanying target and the mobile robot. This paper proposes a companion control strategy based on the Linear Quadratic Regulator (LQR) to enhance the coordination and precision of robot companion tasks. This method enables the robot to adapt to sudden changes in the companion target's motion. Besides, the robot could smoothly avoid obstacles during the companion process. Firstly, a human–robot companion interaction model based on nonholonomic constraints is developed to determine the relative position and orientation between the robot and the companion target. Then, an LQR-based companion controller incorporating behavioral dynamics is introduced to simultaneously avoid obstacles and track the companion target's direction and velocity. Finally, various simulations and real-world human–robot companion experiments are conducted to regulate the relative position, orientation, and velocity between the target object and the robot platform. Experimental results demonstrate the superiority of this approach over conventional control algorithms in terms of control distance and directional errors throughout system operation. The proposed LQR-based control strategy ensures coordinated and consistent motion with target persons in social companion scenarios.

1. Introduction

Human–robot interaction has become an essential characteristic of autonomous robots [1]. As a typical application of human–robot symbiosis, human-following robots have become popular in fields, such as logistics handling [2], rehabilitation assistance [3], and elderly care [4]. This technology can effectively alleviate the strain on medical resources and the rising labor costs associated with an aging population. Human–robot following refers to the ability of a robot to actively respond to the walking behavior of a target person in a dynamically shared environment, maintaining a safe following distance and proactively avoiding obstacles during movement, thereby assisting the target person in completing tasks.

Currently, human–robot following primarily focuses on detecting and tracking the target person, while less emphasis on following control. Achieving safe and stable interactive collaboration in a symbiotic environment relies on practical control algorithms. Furthermore, most studies of the following control strategies concentrate on the trailing mode, where the robot follows behind the person [5]. For example, Sun et al. [6] designed a following control strategy based on the PID control algorithm, which balances the safety and the comfort of the target individual. Peng et al. [7] proposed an impedance-following control strategy based on human–robot companion dynamics. Yuan et al. [8] proposed a control strategy based on artificial potential fields, utilizing forces from potential fields to guide the robot in following the target person while avoiding obstacles. However, studies on human walking behavior indicate that humans prefer walking side-by-side, as this allows the robot to remain within the human's field of vision, thereby achieving higher social acceptance [9,10].

* Corresponding authors.
E-mail addresses: yuhui@fjirsm.ac.cn (H. Yu), dhd@fjirsm.ac.cn (H. Dai).

https://doi.org/10.1016/j.birob.2024.100185

Researchers have extended this finding to human–robot following, proposing that a robot accompanying a person from the side offers a more comfortable and natural interaction [11,12]. To address this, Yao et al. [13] designed a following controller based on the PID algorithm, which switches the robot from trailing to side-following when turning corners. However, this strategy is limited to specific scenarios like corridor corners. Xue et al. [14] proposed a human–robot companion control strategy based on a virtual tracking target. But it converts side-by-side following to trailing, resulting in jerky and inaccurate robot-following trajectories. Morioka et al. [15] and Hu et al. [16] introduced a human–robot companion control based on a virtual spring model to achieve compliant control of the target individual. Nevertheless, the control precision and stability of the virtual spring model are poor, with considerable lag in control response, which can lead to safety issues. To address the shortcomings of the virtual spring model, impedance control, as a typical compliant control method, ensures that the robot actively adapts to human motion changes and maintains smooth robot movement. Tian et al. [17] designed a motion controller model with adjustable impedance control parameters, enabling the robot to actively maintain an appropriate companion space. However, this force control algorithm involves parameters that have complex nonlinear dynamics between each other. Moreover, the companion above control strategies often overlook a critical aspect of human–robot companions: the coordination of movements between the robot and the human.

Motion coordination of human–robot companionship is essential for maintaining the stability of the side-by-side motion formation, which refers to the stable matching of direction and speed between the robot and the target person [18]. In real-world scenarios, human motion is often irregular and dynamically changing, significantly increasing the difficulty for the robot to follow. To ensure the overall stability of the human–robot companion system, the robot must be capable of real-time and accurate perception, as well as fast response to the motion changes of the target person. Therefore, enhancing the motion coordination between the robot and the target person has become a critical issue that needs to be addressed in the research and design of human–robot companion control.

To ensure the safety of human–robot cooperation, robots must have the ability of autonomous obstacle avoidance. Among traditional obstacle avoidance methods, the artificial potential field method [19] is a classic approach widely applied in various scenarios. However, this method is prone to getting trapped in local optima, which can limit its effectiveness. Morioka et al. [15] designed an obstacle avoidance strategy based on the virtual spring model, which achieves obstacle avoidance by establishing virtual spring forces between the robot and obstacles. Nonetheless, this method has a slow response time. However, these previous studies of obstacle avoidance ignored the robots' naturalness in human–robot companions. Tian et al. [17] designed an obstacle avoidance module for following robots using behavioral dynamics, enhancing the naturalness of the robot's obstacle avoidance behavior by simulating human avoidance behavior. They validated the advantages of behavioral dynamics through simulation comparative experiments. As such, the behavioral dynamic is preferred, which enables robot avoidance of obstacles by mimicking human walk behavior. This paper integrated behavioral dynamics into the Linear Quadratic Regulator (LQR) controller to enhance the naturalness of the obstacle avoidance strategy, enabling the robot to avoid obstacles by mimicking human walking behavior.

The main contribution of this paper specifically consists of the following two parts:

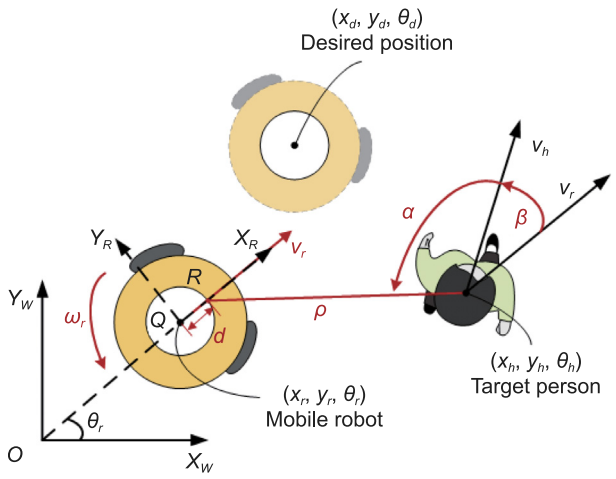

Fig. 1. Kinematics model for the interaction between the accompanying target and the mobile robot.

- This paper proposes a human–robot companion control strategy based on the LQR. The strategy aims to enhance the coordination of human–robot companion motion while ensuring high accuracy and robustness of the control system, thus addressing the deficiencies of other control strategies in motion coordination. The proposed control strategy is compared with traditional control algorithms through simulations and real-world experiments, demonstrating superior control performance on the specified evaluation metrics.
- Firstly, by analyzing the kinematic relationship between the human and the robot during the companion process, the human–robot companion model based on relative distance, relative bearing, and relative heading is established. Secondly, leveraging the state–space equations of the human–robot companion system, the LQR-based companion controller is designed to control the relative pose between humans and robots while tracking the target person's motion speed, thereby improving the motion coordination of the human–robot. Finally, using behavioral dynamics models, an obstacle avoidance strategy for the companion robot is designed to enhance the naturalness of robot obstacle avoidance behavior by simulating human behavior.

2. Human-robot companion model

2.1. Robot kinematics model

In Fig. 1, the human-following robot is a two-wheeled differentially-driven mobile robot. The coordinate systems are defined as follows: X_WOY_W represents the world coordinate system, X_ROY_R represents the robot coordinate system, $Q = [x_r, y_r, \theta_r]$ is the mass center of the robot. Assume that the center of the robot's wheel axle and mass are not aligned on the same horizontal plane. Therefore, we define d as the distance between the robot's wheel axis and its centroid. $R = [x_R, y_R, \theta_R]$ represents the center of the wheel axis. The control input vector $u_r = [v_r, \omega_r]^T$ comprises the robot's linear velocity v_r and angular velocity ω_r. Considering the requirements of physical elements, it is essential to impose reasonable physical constraints on the control inputs of the robot, i.e., $|u_r| \leq u_r^{\max}$, where $u_r^{\max} = [v_r^{\max}, \omega_r^{\max}]^T$ represents the maximum permissible control input values.

The differential-driven mobile robot adheres to nonholonomic constraints [20]. Therefore, its kinematics can be described as

follows:

$$\begin{bmatrix}\dot{x}_r\\ \dot{y}_r\\ \dot{\theta}_r\end{bmatrix}=\begin{bmatrix}cos\theta_r & 0\\ sin\theta_r & 0\\ 0 & 1\end{bmatrix}\begin{bmatrix}v_r\\ \omega_r\end{bmatrix} \tag{1}$$

The position (x_R, y_R) of the reference point R can be expressed by

$$\begin{cases}x_R = x_r + d\cos\theta_r\\ y_R = y_r + d\sin\theta_r\end{cases} \tag{2}$$

2.2. Human-accompanying model

Human–robot companionship refers to the scenario where a robot accompanies a target person, moving in parallel with them and maintaining a certain relative distance and bearing on the person. In Fig. 1, the target person's state is defined as $P_h = [x_h, y_h, \theta_h, v_h, \omega_h]^T$, where (x_h, y_h) and θ_h represent the position and heading angle of the target person, respectively. The terms v_h and ω_h represent the forward and turning velocities of the target person, respectively. Normal human walking motion generally involves no lateral or longitudinal slipping, indicating that human walking motion is subject to nonholonomic constraints. Thus, the human-walking motion model [20] can be defined as:

$$\begin{cases}\dot{x}_h = \dot{v}_h\cos\theta_h\\ \dot{y}_h = \dot{v}_h\sin\theta_h\\ \dot{\theta}_h = \omega_h\end{cases} \tag{3}$$

Moreover, we define the state variables of the human–robot companion system as $\chi = [\rho, \alpha, \beta]^T$.

The relative distance between the reference point R and the target person is denoted as ρ, where $\rho = \sqrt{\rho_x^2 + \rho_y^2}$. Based on the geometric positional relationship between the mobile robot and the target person, the projections of ρ on the X-axis and Y-axis of the $X_W O Y_W$ can be obtained as ρ_x and ρ_y, respectively, as

$$\begin{cases}\rho_x = x_h - x_R = -\rho\cos(\alpha+\theta_h)\\ \rho_y = y_h - y_R = -\rho\sin(\alpha+\theta_h)\end{cases} \tag{4}$$

The bearing angle α represents the angle between the target person's forward direction and the line between the robot and the target person, as

$$\alpha = \pi + arctan(\rho_y/\rho_x) - \theta_h \tag{5}$$

The orientation angle β indicates the heading angle deviation between the robot and the target person, it can be described as

$$\beta = \theta_h - \theta_r \tag{6}$$

The desired state of the human-accompanying system is denoted as $\chi_d = [\rho_d, \alpha_d, \beta_d]^T$. Here, ρ_d represents the desired companion distance, while $\alpha_d = \pi/2$ or $\alpha_d = 3\pi/2$ denote the robot's position on the target person's left and right sides, respectively. Additionally, setting $\beta_d = 0$ ensures that the robot can promptly respond to changes in the target person's movement direction. Based on the relative pose relationship between the robot and the target person, as well as kinematic equations (1) and (2), the human–robot companion model can be derived as follows:

$$\dot{\chi} = \left[\dot{\rho}, \dot{\alpha}, \dot{\beta}\right]^T \tag{7}$$

where

$$\begin{cases}\dot{\rho} = v_r\cos\gamma - v_h\cos\alpha_r + d\omega_r\sin\gamma\\ \dot{\alpha} = \frac{1}{\rho}\left(v_h\sin\alpha_r - v_r\sin\gamma + d\omega_r\cos\gamma\right) - \omega_h\\ \dot{\beta} = \omega_h - \omega_r\\ \gamma = \alpha_d + \beta_d\end{cases}$$

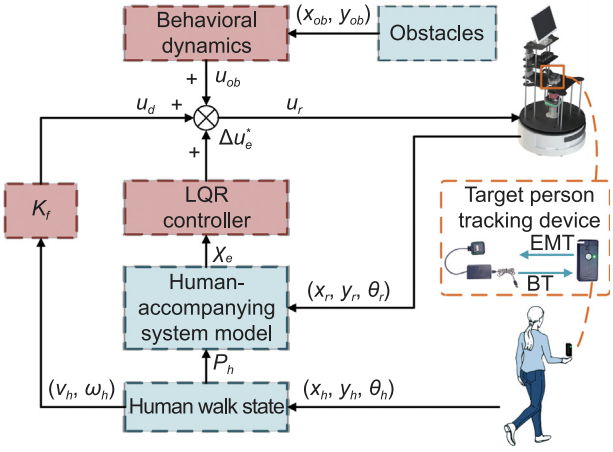

Fig. 2. Schematic diagram of the LQR-based human-accompanying controller.

By applying the Taylor series expansion and the forward Euler method to linearize and discretize the system model (7), the following linear time-varying discrete state–space equations are obtained:

$$\chi_e(k+1) = \tilde{A}(k)\chi_e(k) + \tilde{B}(k)u_e(k) \tag{8}$$

where $\chi_e = \chi - \chi_d = [\rho - \rho_d, \alpha - \alpha_d, \beta - \beta_d]^T$ represents the error between the actual value and the desired value of the system state, $u_e = [v - v_h, \omega - \omega_h]^T$ represents the control input deviation, the sampling period T and k represent the time step in the operation system.

$$\tilde{A} = \begin{bmatrix}1 & a_{12} & a_{12}\\ a_{21} & a_{22} & a_{23}\\ 0 & 0 & 1\end{bmatrix}, \tilde{B} = \begin{bmatrix}T\cos\gamma & Tdsin\gamma\\ \frac{T}{\rho_d}sin\gamma & \frac{T}{\rho_d}dcos\gamma\\ 0 & -T\end{bmatrix}$$

$$\begin{cases}a_{12} = -Tv_hsin\gamma + v_hsin\alpha_d + d\omega_hcos\gamma\\ a_{13} = -T\left(v_hsin\gamma + dw_hcos\gamma\right)\\ a_{21} = -\frac{T}{\rho_d^2}\left[v_hsin\alpha_d - v_hsin\gamma + dw_hcos\gamma\right]\\ a_{22} = \frac{T}{\rho_d}\left[v_hcos\alpha_d - v_dcos\gamma - dw_dsin\gamma\right] + 1\\ a_{23} = -\frac{T}{\rho_d}\left[v_dcos\gamma + dw_dsin\gamma\right]\end{cases}$$

3. LQR-based human-accompanying controller

3.1. Control system design scheme

Human–robot companion control aims to accurately regulate the relative pose between the robot and the target person. To ensure motion coordination in human–robot companionship, the robot must stably accompany variations in the target person's motion speed and direction. Furthermore, the robot must autonomously evade obstacles throughout the human–robot companion process to guarantee the target person's safety. Hence, the above control objectives can be delineated as follows:

$$\lim_{t\to+\infty}|\chi - \chi_d| = 0,\ \lim_{t\to+\infty}|u_r - u_h| = 0,\ \rho_{ob} < \rho_o \tag{9}$$

where $u_r = [v_r, \omega_r]^T$, ρ_{ob} represents the relative distance between the robot and the obstacle, ρ_o represents the influence range of the obstacle.

The proposed human–robot companion control strategy based on the LQR is illustrated in Fig. 2. The human–robot companionship model is derived from the motion state of the target person and the kinematic equations of the robot outlined in the previous section. Based on this model, the cost function of

the LQR is designed as a quadratic integral of the system state error and control input deviation. This approach facilitates precise control of the robot's position while ensuring stable tracking of the target person's motion variations. An obstacle avoidance strategy is devised using behavioral dynamics, enabling mapless navigation for accompanying and avoiding obstacles. Additionally, this study employs an electromagnetic localization module to acquire the pose information of the target person. This module offers 360° surround detection, unaffected by obstacles or environmental lighting conditions, presenting advantages over commonly used detection methods such as laser scanners and stereo vision systems.

3.2. LQR-based human–robot companion controller

We define the output of the human–robot companion controller as follows:

$$u_r(k) = u_d(k) + u_e(k) \tag{10}$$

where $u_d(k)$ and $u_e(k)$ are the feedforward controller and the feedback controller respectively. The feedforward controller can drive the robot to follow the target person without initial state errors and effectively enhance the system's response speed and track accuracy. It is designed as $u_d = K_f u_h$, where K_f represents the gain and u_h represents the target person's velocity. To achieve the optimal motion coordination of the system, the expected speed of the accompanying robot must be consistent with the target person. Thus, $K_f = 1$, indicates the feedforward control output is equal to $u_d = [v_h, w_h]^T$.

LQR is an optimal control strategy based on state feedback, known for its robustness, stability, and ease of implementation. It enables robots to achieve optimal motion control effects while meeting specific performance criteria. Therefore, designing the feedback control loop based on the LQR control strategy enhances the system's control precision and human–robot motion coordination [21]. To further improve the naturalness of the accompanying control, An improved augmented state matrix is defined:

$$\xi(k) = \begin{bmatrix} \chi_e(k) \\ u_e(k-1) \end{bmatrix} \in R^{(m+n)\times 1} \tag{11}$$

where $n = 2$ and $m = 3$ represent the dimensions of the control input and the robot's state variables, respectively. A new augmented state–space equation can be expressed as follows:

$$\begin{cases} \xi(k+1) = \bar{A}\xi(k) + \bar{B}\Delta u_e(k) \\ \eta(k) = \bar{C}\xi(k) \end{cases}$$
$$\Delta u_e(k) = u_e(k) - u_e(k-1) \in \mathbb{R}^{m\times 1}$$
$$\bar{A} = \begin{bmatrix} \tilde{A} & \tilde{B} \\ 0 & I \end{bmatrix} \in \mathbb{R}^{(m+n)\times(m+n)} \tag{12}$$
$$\bar{B} = \begin{bmatrix} \tilde{B} \\ I \end{bmatrix} \in \mathbb{R}^{(m+n)\times m}$$
$$\bar{C} = \begin{bmatrix} I & 0 \end{bmatrix} \in \mathbb{R}^{n\times(m+n)}$$

According to Eq. (9), the cost function of LQR is defined as

$$J = \sum_{k=1}^{N} \left(\xi^T Q \xi + \Delta u_e^T R \Delta u_e\right) \tag{13}$$

where Q is the state weighting matrix, and R is the control input weighting matrix. The first term represents the state error of the human–robot companion system, used to achieve accurate control of the robot's companion position and to track the target person's movement direction. The second term represents the change in the robot's tracking speed of the target person during the human–robot companionship process.

Solve the cost function (13) to obtain the optimal control, as:

$$\Delta u_e^* = -K\xi, \quad K \in \mathbb{R}^{m\times(m+n)} \tag{14}$$

where $K = \left(R + \bar{B}^T P \bar{B}\right)^{-1} \bar{B}^T P \bar{A}$ is the optimal gain matrix that minimizes the cost function, P is a symmetric positive semi-definite matrix that can be obtained by solving the Riccati equation [22]. The general form of the Riccati equation is as follows:

$$P = \bar{A}^T P \bar{A} - \bar{A}^T P \bar{B}\left(R + B^T \bar{P} B\right)^{-1} \bar{B}^T P \bar{A} + Q \tag{15}$$

Based on Eqs. (14) and (15), the system's optimal control output Δu_e^* can be obtained. Substituting this into Eqs. (10) and (12) yields the optimal control output for the human–robot companion system:

$$u_r^*(k) = u_d(k) + u_e(k-1) - K\xi \tag{16}$$

The human–robot accompanying system can obtain the optimal control output through the above steps.

3.3. Obstacle avoidance based on behavioral dynamics

Natural obstacle avoidance capability requires the robot's obstacle avoidance behaviors to be closer to human's natural behaviors. Current obstacle avoidance methods often ignore human–robot interaction factors and neglect the naturalness of the interaction process, which negatively impacts the social acceptability of robots. To enhance the naturalness of robot obstacle avoidance behavior during human–robot interactions, Fajen et al. [23] have studied human avoidance behavior. It has been found that both the direction and distance of obstacles relative to a person jointly influence human avoidance behavior. Specifically, humans primarily adjust their direction of movement to bypass obstacles, with minimal adjustment to their walking speed. Furthermore, the angular acceleration of human turning increases as the obstacle's azimuth angle decreases and the distance to the obstacle decreases. This approach can effectively improve the naturalness of robot obstacle avoidance. Furthermore, Tian et al. [17] experimentally validated the effectiveness of this method in human–robot companion obstacle avoidance. Therefore, this paper will apply a companion robot control strategy by combining obstacle avoidance based on behavior dynamics with the LQR controller.

We define the relative distance between the robot and the obstacle as ρ_{ob}. The influence range of the obstacle is defined as $\rho_o = r_o/K_{ob}$, where r_o is the actual radius of the obstacle and K_{ob} is the ratio of the obstacle size to its influence range. When $\rho_{ob} < \rho_o$, it indicates that the robot has entered the obstacle's influence range. At this time, the obstacle avoidance output for a single obstacle is:

$$\Lambda_{ob} = -\eta\phi e^{-c_1|\phi|} e^{-c_2\rho_{ob}} \tag{17}$$

where Λ_{ob} is the angular acceleration of the robot's obstacle avoidance output, ϕ is the bearing angle of the obstacle in the $X_R O Y_R$ coordinate system, η is the robot's obstacle avoidance gain coefficient; c_1 is the obstacle bearing angle gain coefficient, c_2 is the obstacle distance gain coefficient. Therefore, the obstacle avoidance output can be defined as

$$\dot{u}_{obi} = [0, \Lambda_{obi}]^T \tag{18}$$

where the subscript i represents the index of obstacles within the obstacle avoidance function's operating range. Integrating $\dot{u}_{obi}$ yields the avoidance output matrix u_{obi}. When the robot is affected by N_{ob} obstacles, the angular velocity control outputs

Table 1
Experimental parameters.

Parameters	Value
Robot mass	40 kg
Wheel radius	0.07 m
Moment of inertia	0.08 (kg·m^2)
Sample period	0.05 s
Q	$[25, 10, 25, 30, 30]^T$
R	$[20, 20]^T$
η	28
c_1	1.5
c_2	0.9
K_{ob}	0.6
ρ_d	1 m
d	0.25 m
$u_r^{\max}$	$[1.5$ m/s, 0.5π rad/s$]^T$

generated by multiple obstacles can be summed to form the output of the obstacle avoidance controller.

$$u_{ob} = \sum_{i=0}^{N_{ob}} u_{obi} \tag{19}$$

Combining Eqs. (16) and (18), the final control input based on LQR and behavior dynamics for human–robot companionship and obstacle avoidance strategy is

$$u_r(k) = u_d(k) + u_e(k\text{-}1) - K\xi + u_{ob} \tag{20}$$

4. Simulations and experiments

4.1. Evaluation setup

The proposed companion control strategy was validated through both simulation and real-world experiments. A set of evaluation metrics was designed to assess the controller's performance quantitatively. The simulation and real-world experiments were conducted using the same experimental parameters, as shown in Table 1.

To quantitatively evaluate the control accuracy, smoothness of control output, and coordination of human–machine accompanying movement for the proposed accompanying control strategy, we define the following two evaluation metrics:

$$RMSE = \sqrt{\frac{1}{T_{task}} \sum_{t=0}^{T_{task}} [\chi(t) - \chi_d(t)]^2} \tag{21}$$

where, T_{task} represents the system operation time, $\chi(t)$ and $\chi_d(t)$ denote the actual state of the robot and the desired state at time t, respectively. $RMSE$ is the root mean square error of $[\rho, \alpha, \beta]$. This metric evaluates the accuracy of the system state variables during the robot control process. The state variables ρ, α, and β will be assessed in subsequent measurements. Meanwhile, we use the root mean square error of velocity (RMSV) to quantify the velocity-tracking performance of the proposed method.

$$RMSV = \sqrt{\frac{1}{T_{task}} \sum_{t=1}^{T_{task}} (u_t - u_d)^2} \tag{22}$$

where u_t represents the input of the robot at time t, and u_d is the desired companion velocity, which is the instantaneous speed of the target person. This metric is used to evaluate the smoothness of the control output and the robot's motion coordination with the target person's velocity.

4.2. Simulation results

To validate the effectiveness of the proposed method, a simulation experiment was designed in Fig. 3. The target person starts from (3,3) and moves along the positive direction of the X-axis, as indicated by the red trajectory in Fig. 3(a). Several different starting points and initial poses were assigned to the robots to execute either left-side or right-side companionship. The robot's starting points were set at (3,6), (0,5), (0,3), (0,1), and (3,0), as indicated by the dashed trajectories in Fig. 3(a). The same color trajectory indicates the same starting point but different initial heading angles. Fig. 3(b) and (c) show the error curves of the human–robot companion system state variables, with the colors of these curves corresponding to their respective trajectories. The results indicate that robots starting from different initial states can effectively achieve human–robot companionship, with the relative distance, relative bearing, and relative heading angle between the robot and the target person quickly converging to the desired values, preliminarily validating the effectiveness of the proposed companion control strategy.

To further verify the comprehensive performance of the companion control strategy, we designed an eight-shape trajectory with both variable speed and direction. The equation of this trajectory is

$$\begin{cases} x(t) = \frac{10\sin(t)\cos(t)}{1+\sin^2(t)} + 5 \\ y(t) = \frac{6\cos(t)}{1+\sin^2(t)} - 3 \end{cases} \tag{23}$$

As shown in Fig. 4(a), the target person moves along an 8-shaped trajectory, starting at (5,2), with time-varying linear and angular velocities to simulate dynamic changes in the real world. An obstacle, represented by a gray solid circle, is positioned at (5.1,−1.8) with a radius of 0.15 m, and its influence range is indicated by the gray dashed circle with a radius of 0.4 m. The robot started the companionship task from the right side of the target person. Additionally, the proposed LQR-based companion control strategy was compared with control methods based on PID, Virtual Spring Model (VSM), and Impedance Control (IC).

In Fig. 4(a), the purple trajectory represents the robot's path using the proposed LQR-based companion control strategy, while the green, yellow, and pink trajectories represent the paths using IC, PID, and VSM control methods, respectively. Fig. 4(d) shows the robot's relative distance to the obstacle and the obstacle avoidance control output curve based on behavioral dynamics, with the purple dashed line indicating the obstacle's influence range. When the robot enters the obstacle's influence range, the behavioral dynamics-based obstacle avoidance component responds by generating an avoidance control signal to adjust the robot's angular velocity and steer around the obstacle. Fig. 4(b) presents the error curves of the human–robot companion system state variables. During obstacle avoidance, the PID, VSM, and IC methods exhibit large steady-state errors and significant fluctuations in system state variables. Although all three methods can control the robot's accompanying pose relative to the human, they fail to effectively stabilize the system state under significant disturbances, such as deviations caused by obstacle avoidance, leading to system oscillations. In contrast, the proposed control strategy demonstrates higher accuracy and stability. Even when significant deviations occur during obstacle avoidance, the system state quickly reconverges, with smaller deviations and fluctuations than other methods.

Fig. 4(c) illustrates the curves of the velocity variation curves of the robot and the target person. The black dotted lines indicate the linear and angular velocity constraints. Under fixed parameter simulation conditions, the VSM, PID, and IC methods also effectively track the target person's speed. However, these methods exhibit significant oscillations and slow speed recovery during obstacle avoidance. In contrast, when employing the LQR-based companion control strategy, the robot smoothly tracks the target person's speed changes.

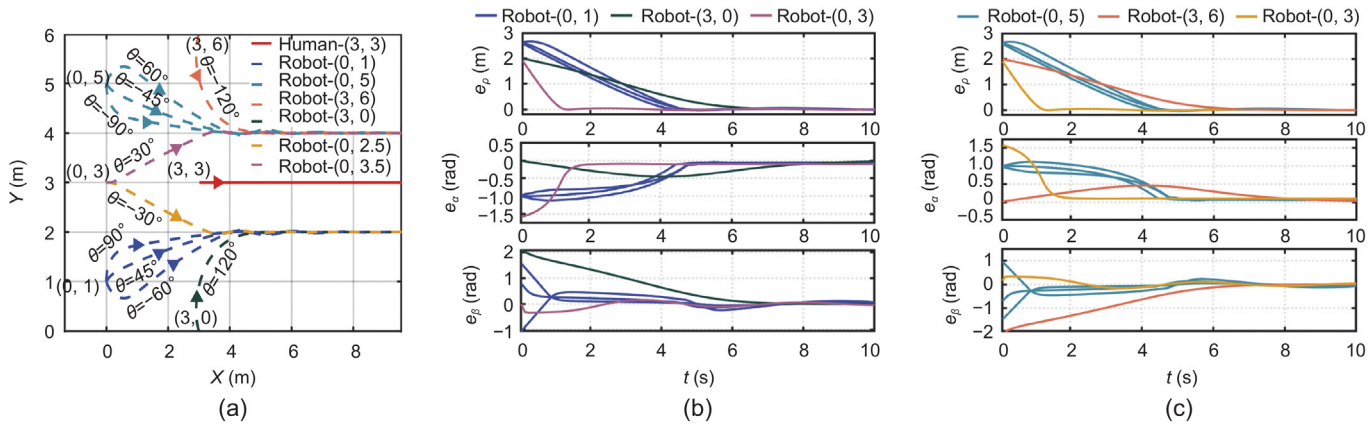

Fig. 3. Human–robot accompanying simulation experiment. The target person moved in a straight line trajectory along $Y = 3$; the robot achieved stable accompanying following at each starting point. (a) Trajectories. (b) Right trajectories state error. (c) Left trajectories state error.

Table 2
Quantitative simulation results of human–robot accompanying without obstacles and abrupt changes in the person's motion.

Trajectory	Method	*RMSE*			*RMSV*	
		ρ (cm)	α (rad)	β (rad)	v (m/s)	ω (mrad/s)
Linear	**LQR**	**0.001**	**0.005**	**0.000**	**0.001**	**0.016**
	PID	0.281	0.075	0.000	0.009	0.028
	VSM	3.743	0.269	0.000	0.097	0.036
	IC	4.371	0.094	0.000	0.184	0.020
8-shaped	**LQR**	**5.123**	**0.012**	**0.021**	**0.072**	**5.539**
	PID	5.579	0.068	0.031	0.175	5.555
	VSM	13.873	0.380	0.135	0.077	35.750
	IC	7.801	0.093	0.051	0.08	7.910
Circle	**LQR**	**0.038**	**0.006**	**0.003**	**0.050**	**0.773**
	PID	2.411	0.076	0.023	0.100	8.541
	VSM	1.612	0.215	0.068	0.098	9.795
	IC	3.410	0.096	0.021	0.087	6.541

Fig. 4(d) presents the obstacle avoidance output component curve and the robot-obstacle relative distance curve. It can be observed that when the distance between the robot and the obstacle was less than the obstacle's influence range, an angular acceleration component was generated. Even during obstacle avoidance, where the superimposed effect of the avoidance output caused significant fluctuations in the robot's angular velocity, the strategy responded quickly, enabling the system to reconverge to the desired state rapidly. This comparison underscored the advantages of the proposed LQR-based companion control strategy in motion coordination performance and stability, demonstrating its superior suitability for handling dynamic changes in complex environments compared to other methods.

Additionally, we conducted repeated companion simulation experiments with straight and circular target person trajectories, and the quantitative evaluation results are shown in Table 2. Compared to other traditional algorithms, the proposed strategy shows significant improvements in the accuracy evaluation metrics *RMSE* and *RMSV*.

Compared to traditional control methods, the above simulation results validate that the proposed control strategy ensures higher accuracy of system state variables and more precise tracking of the target's speed. In the simulation experiments with complex trajectories, the proposed control strategy, under ideal conditions, improves the RMSE of ρ, α, and β by at average 35.86%, 88.76%, and 58.51%, respectively, and the RMSV of v and ω by at average 25.12% and 38.27%, respectively, demonstrating the excellent motion coordination of the proposed control strategy.

4.3. Real-world experiments results

To further validate the effectiveness of the proposed method on a real robotic platform, we built an experimental setup as shown in Fig. 5. Within the same local area network, we deployed the algorithm computation on a laptop running MATLAB and the execution on the robot's onboard computer running the Robot Operating System (ROS) through a master–slave communication mode. The ROS data collection node receives control commands from the algorithm computation side and drives the differential robot chassis for companion motion. Additionally, an electromagnetic tracking positioning sensor (Amfitech, Gen2, Denmark) is installed on the robot as the signal transmitter, while the target person wears the receiver. Based on the magnetic dipole model, the alternating magnetic field generated by the transmitter is analyzed, and the 3D pose data of the companion object is transmitted via Bluetooth to the robot. The electromagnetic signal can penetrate the human body, allowing stable tracking of the target person's pose even when obstacles are present. The receiver is integrated into the robot to receive signals from the transmitter.

Depending on the application scenario, different sensing modules are used for obstacle position acquisition. The VICON optical motion capture system ((Oxford Metrics Limited, Vero2.2, UK)) is used in indoor experimental settings. The robot is equipped with infrared reflective markers recognizable by the VICON system, enabling environmental perception and precise recording of human–robot trajectories and obstacle positions. In outdoor environments, a laser radar (Pepperl+Fuchs, R2000, Germany) can detect obstacles and record the robot's real-time position through odometry.

In the first set of experiments, the target person walks along a U-shaped trajectory within a global map, as shown in Fig. 6(a). These experiments validate the motion coordination performance of the robot's autonomous companionship. The target person's speed accelerates and decelerates along the two straight segments, while at the turning points, the target person performs approximately circular curved motions. Fig. 6(b) describes the accuracy of the robot in system error correction. Even when deviations occur due to abrupt changes in the target person's movement, the control system quickly reconverges, minimizing the system state error and maintaining stability. Combined with the LQR simulation data for straight and circular trajectories shown in Table 2, this control strategy demonstrates high control accuracy.

By evaluating the robot's performance in real-world scenarios, these experiments confirm that the proposed LQR-based companion control strategy can effectively maintain motion coordination

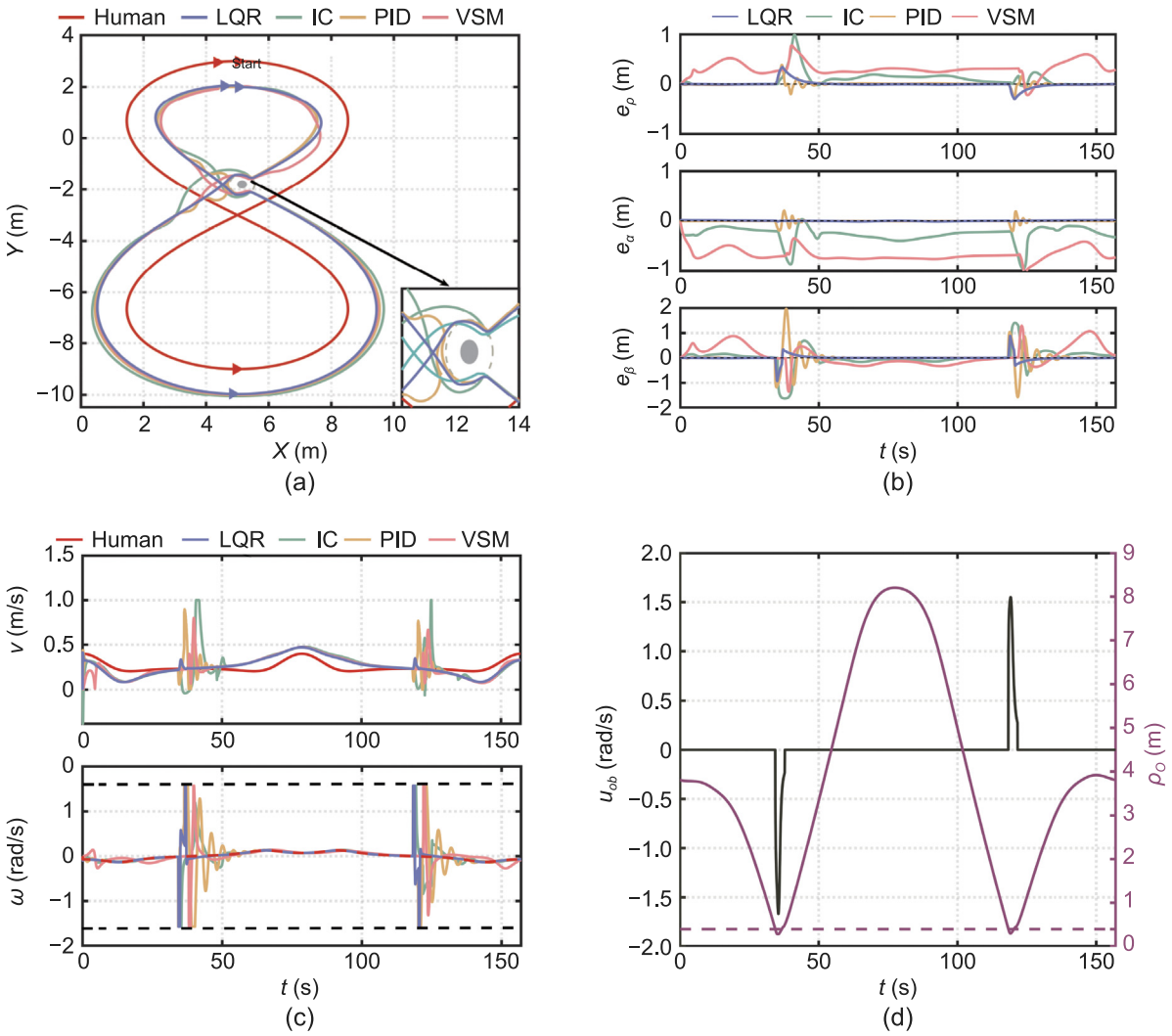

Fig. 4. 8-Shaped trajectory experiment with obstacles for the human-accompanying robot in simulations. (a) Trajectories. (b) State error. (c) Control inputs. (d) u_{ob} to ρ_o relationship.

and system stability, ensuring accurate and smooth tracking of the target person's movement.

Furthermore, Fig. 6(c) illustrates that throughout the experiment, the robot successfully adapted to the target person's movement changes and maintained smooth speed tracking within the speed constraint $\pm u_r^{max}$. Due to the randomness of human movement, the target person's speed curve tended to fluctuate during the experiment. However, the robot responded quickly and accompanied the target person at the expected speed. The robot's companion motion remained relatively stable, with results similar to the simulation's *RMSV*. The chart results indicate that this control strategy allows the robot to track the target person stably while maintaining accuracy, and achieving good motion coordination. This real-world validation complements the simulation data, highlighting the effectiveness of the proposed LQR-based companion control strategy in dynamic environments. The robot quickly adjusts to speed variations and trajectory changes, ensuring seamless and stable companion movement. This aligns with the intention to enhance human–robot interaction by providing precise control and smooth motion coordination, which is essential for practical applications.

To further validate the performance of the proposed control strategy in complex scenarios, we conducted an experiment where the target person followed an 8-shaped trajectory similar to the one used in the simulation. As shown in Fig. 7(a), the target's walking path approximates an inverted 8-shaped, with cylindrical obstacles of radius $r_o = 0.4875$ m placed at coordinates (1.75, −9) and (5.15, −1.6), giving an obstacle influence range of $\rho_o = 1.3$ m. Furthermore, as shown in Fig. 7(d), at times $t_1 = 10.3$ s and $t_2 = 30.85$ s, the distance between the robot and the obstacles is completely within the influence range, i.e., $\rho_{ob} < \rho_o$. At these points, the robot simultaneously performs obstacle avoidance while carrying out the companion task.

The system state error curves are shown in Fig. 7(b). Apart from significant errors at t_1 and t_2 during obstacle avoidance and turning points, the system error remains minimal throughout the experiment, fluctuating around the expected zero value, demonstrating system state accuracy.

Fig. 7(c) illustrates the control output. During the obstacle avoidance and turning at t_1 and t_2, , there are sharp changes in angular velocity. At other times, the robot maintains stable companion motion while ensuring safe speed, demonstrating good speed-tracking performance in obstacle avoidance scenarios.

This experiment confirms that the proposed LQR-based control strategy maintains high accuracy in system state variables and ensures stable speed tracking and practical obstacle avoidance. The robot's ability to quickly adapt to dynamic changes and maintain smooth motion coordination is crucial for practical applications in complex environments.

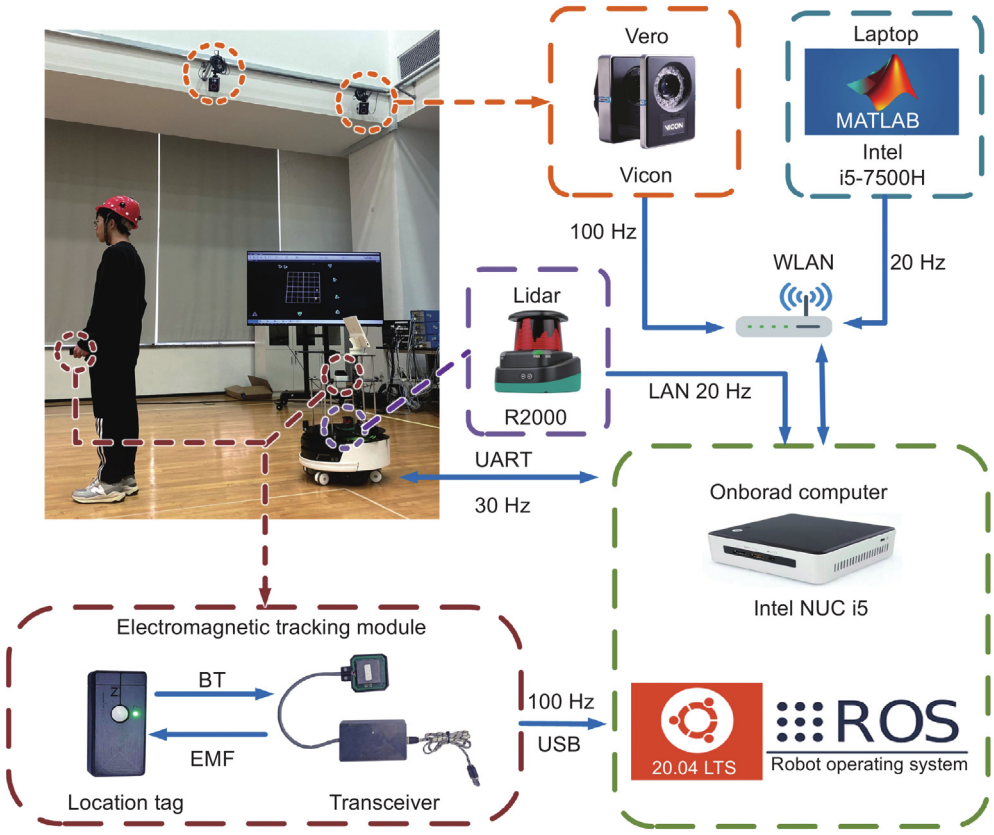

Fig. 5. Experiment setup for the human-accompanying system.

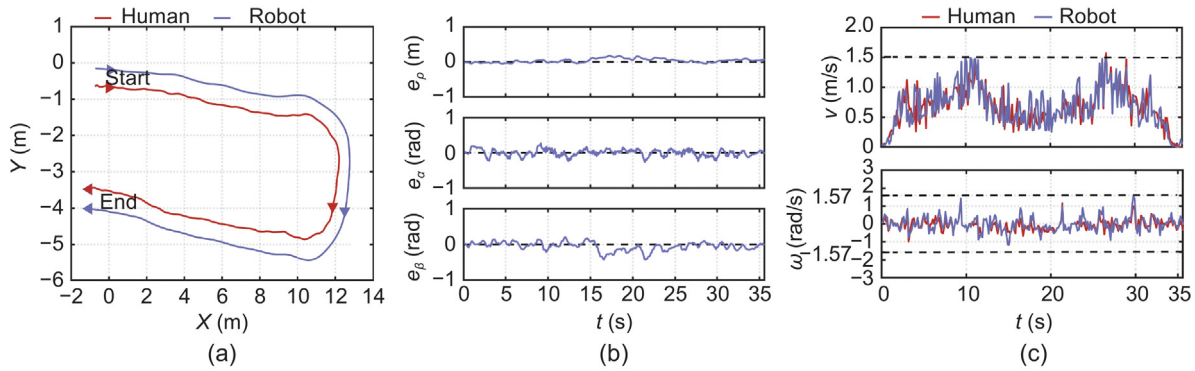

Fig. 6. Experiment of the robot human-accompanying along a U-shaped trajectory in an obstacle-free environment. (a) Trajectories. (b) State error. (c) Control inputs.

The evaluation metrics results from the two real-world experiments (21)(22) are shown in Table 3. According to these results, the robot under the proposed control strategy can effectively adapt to sudden movements of the target person, maintaining smooth and stable speed tracking with high accuracy. Even when the target's speed changes abruptly or when significant deviations in the system state occur due to environmental disturbances, the robot can quickly adjust and bring the system state error back to the set value. This demonstrates that the proposed control strategy has good motion coordination in real-world application scenarios.

Table 3
Results of the physical experiment results.

Trajectory	*RMSE*			*RMSV*	
	ρ (m)	α (rad)	β (rad)	v (m/s)	ω (rad/s)
U-shaped	0.068	0.094	0.130	0.245	0.245
8-shaped	0.226	0.324	0.142	0.285	0.241

5. Conclusion

This paper proposed a companion robot control strategy for tracking a target person in human–robot interaction scenarios while enabling the robot to avoid obstacles autonomously. A kinematic model of the companion robot system was established based on a differential drive mobile robot experimental platform, and the system state variables for the companion process were defined. An LQR-based algorithm was developed to design the companion system controller, ensuring that the robot could maintain a stable and accurate relative position to the target while adapting to changes in the target's movement direction

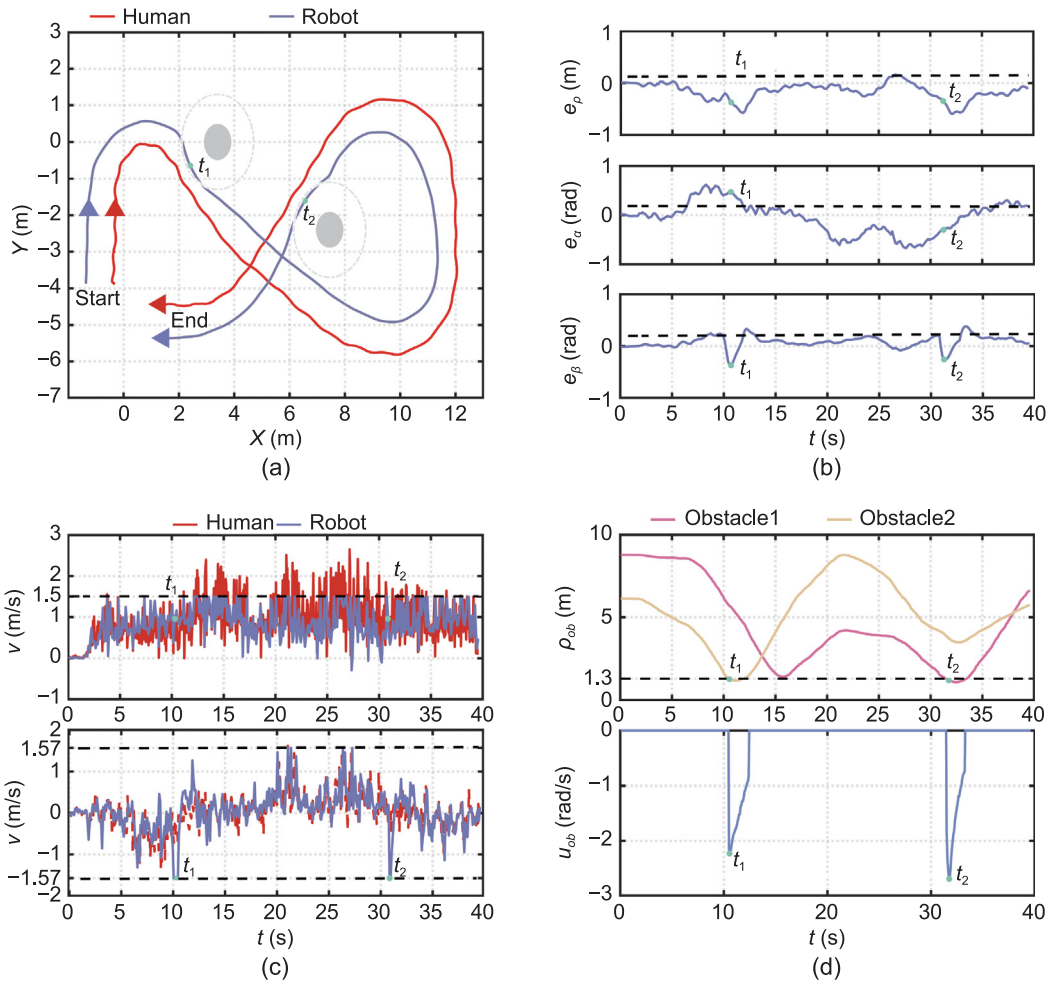

Fig. 7. Experiment of the human–robot companionship along an 8-shaped trajectory in an environment obstacles. (a) Trajectories. (b) State error. (c) Control inputs. (d) u_{ob} to ρ_o relationship.

and speed. To address the need for the robot to navigate complex environments during the companion process, the control strategy integrated a behavior dynamics-based obstacle avoidance approach that mimicked natural human obstacle avoidance behaviors. Initial validation of the proposed control strategy's performance in human–robot companionship was conducted in a simulation environment. Under ideal simulation conditions, compared to other control strategies, the RMSE of ρ, α, and β by at average 35.86%, 88.76%, and 58.51%, respectively, and the RMSV of v and ω by at average 25.12% and 38.27%, respectively, demonstrating the excellent motion coordination of the proposed control strategy. Comparative experiments demonstrated that the proposed strategy outperformed the Proportional PID, VSM, and IC methods in terms of accuracy and coordination of human–robot movement. Additionally, the feasibility of the control strategy was quantitatively evaluated through obstacle avoidance experiments on a real-world experimental platform.

In the control module, due to the strict parameter tuning requirements of the LQR, neural networks will be employed for parameter optimization to achieve adaptive parameter tuning. In the decision-making module, since the desired state of the companion system is manually set and cannot adapt to sudden narrow terrains, strategies that consider environmental information will be added for adaptive decision-making. These improvements aim to enhance the practicality of the companion control algorithm in complex application scenarios.

CRediT authorship contribution statement

Zefan Su: Writing – review & editing, Writing – original draft, Visualization, Validation, Software, Project administration, Methodology, Data curation, Conceptualization. **Hanchen Yao:** Writing – review & editing. **Jianwei Peng:** Conceptualization. **Zhelin Liao:** Data curation. **Zengwei Wang:** Data curation. **Hui Yu:** Writing – review & editing. **Houde Dai:** Writing – review & editing, Visualization, Validation. **Tim C. Lueth:** Writing – review & editing.

Declaration of competing interest

The authors declare that they have no known competing financial interests or personal relationships that could have appeared to influence the work reported in this paper.

Acknowledgments

This work was supported in part by the National Natural Science Foundation of China (61973293), the Fujian Provincial Science and Technology Plan Project (2023T3008, 2023T3069, and 2023T3084), the Quanzhou Science and Technology Plan Project (2022FX7), the Open Project Program of Fujian Key Laboratory of Special Intelligent Equipment Measurement and Control (FJIES2023KF02).

References

[1] S.S Honig, T. Oron-Gilad, H. Zaichyk, V. Sarne-Fleischmann, S. Olatunji, Y. Edan, Toward socially aware person-following robots, IEEE Trans. Cogn. Dev. Syst. 10 (4) (2018) 936–954.

[2] M.J. Islam, J. Hong, J. Sattar, Person-following by autonomous robots: A categorical overview, Int. J. Robot. Res. 38 (14) (2019) 1581–1618.

[3] Q.Y. Yan, J. Huang, Z.H. Yang, Y. Hasegawa, T. Fukuda, Human-following control of cane-type walking-aid robot within fixed relative posture, IEEE/ASME Trans. Mechatronics 27 (1) (2021) 537–548.

[4] S. Li, K. Milligan, P. Blythe, Y.H.Z. Zhang, S. Edwards, N. Palmarini, L. Corner, Y.J. Ji, F. Zhang, A. Namdeo, Exploring the role of human-following robots in supporting the mobility and wellbeing of older people, Sci. Rep. 13 (1) (2023) 6512.

[5] N.V. Toan, M.D. Hoang, P.B. Khoi, S.-Y. Yi, The human-following strategy for mobile robots in mixed environments, Robot. Auton. Syst. 160 (2023) 104317.

[6] Y. Sun, L. Sun, J.T. Liu, Human comfort following behavior for service robots, in: 2016 IEEE International Conference on Robotics and Biomimetics, ROBIO, IEEE, 2016, pp. 649–654.

[7] J.W. Peng, Z.L. Liao, Z.F. Su, H.C. Yao, Y.D. Zeng, H.D. Dai, Human-robot interaction dynamics-based impedance control strategy for enhancing social acceptance of human-following robot, in: 2023 China Automation Congress, CAC, IEEE, 2023, pp. 7354–7360.

[8] J. Yuan, S.M. Zhang, Q.X. Sun, G.D. Liu, J.X. Cai, Laser-based intersection-aware human following with a mobile robot in indoor environments, IEEE Trans. Syst. Man Cybern.: Syst. 51 (1) (2018) 354–369.

[9] M. Costa, Interpersonal distances in group walking, J. Nonverbal Behav. 34 (2010) 15–26.

[10] E. Repiso, A. Garrell, A. Sanfeliu, Adaptive side-by-side social robot navigation to approach and interact with people, Int. J. Soc. Robot. 12 (4) (2020) 909–930.

[11] Y. Morales, S. Satake, R. Huq, D. Glas, T. Kanda, N. Hagita, How do people walk side-by-side? Using a computational model of human behavior for a social robot, in: Proceedings of the 7th Annual ACM/IEEE International Conference on Human-Robot Interaction, 2012, pp. 301–308.

[12] Y. Morales, T. Kanda, N. Hagita, Walking together: Side-by-side walking model for an interacting robot, J. Hum.-Robot Interact. 3 (2) (2014) 50–73.

[13] H.C. Yao, H.D. Dai, E.H. Zhao, P.H. Liu, R. Zhao, Laser-based side-by-side following for human-following robots, in: 2021 IEEE/RSJ International Conference on Intelligent Robots and Systems, IROS, IEEE, 2021, pp. 2651–2656.

[14] G. Xue, H.C. Yao, Y.C. Zhang, J.Y. Huang, L.Q. Zhu, H.D. Dai, UWB-based adaptable side-by-side following for human-following robots, in: 2022 IEEE International Conference on Robotics and Biomimetics, ROBIO, IEEE, 2022, pp. 333–338.

[15] K. Morioka, J.-H. Lee, H. Hashimoto, Human-following mobile robot in a distributed intelligent sensor network, IEEE Trans. Ind. Electron. 51 (1) (2004) 229–237.

[16] J.-S. Hu, J.-J. Wang, D.M. Ho, Design of sensing system and anticipative behavior for human following of mobile robots, IEEE Trans. Ind. Electron. 61 (4) (2013) 1916–1927.

[17] H.Y. Tian, X. Ma, Behavioral dynamics-based impedance control for collision avoidance of human-following robots, in: 2022 IEEE International Conference on Real-Time Computing and Robotics, RCAR, IEEE, 2022, pp. 349–354.

[18] E. Prassler, D. Bank, B. Kluge, Motion coordination between a human and a mobile robot, in: IEEE/RSJ International Conference on Intelligent Robots and Systems, Vol. 2, IEEE, 2002, pp. 1228–1233.

[19] O. Khatib, Real-time obstacle avoidance for manipulators and mobile robots, Int. J. Robot. Res. 5 (1) (1986) 90–98.

[20] G. Arechavaleta, J.-P. Laumond, H. Hicheur, A. Berthoz, On the nonholonomic nature of human locomotion, Auton. Robots 25 (2008) 25–35.

[21] D.D. Zhao, X.D. Yang, Y.C. Li, L. Xu, J.H. She, S. Yan, A Kalman–Koopman LQR control approach to robotic systems, IEEE Trans. Ind. Electron. (2024).

[22] S. Zoboli, V. Andrieu, D. Astolfi, G. Casadei, J.S Dibangoye, M. Nadri, Reinforcement learning policies with local LQR guarantees for nonlinear discrete-time systems, in: 2021 60th IEEE Conference on Decision and Control, CDC, IEEE, 2021, pp. 2258–2263.

[23] B.R. Fajen, W.H. Warren, Behavioral dynamics of steering, obstable avoidance, and route selection, J. Exp. Psychol.: Hum. Percept. Perform. 29 (2) (2003) 343.